Supplementary Figure 1

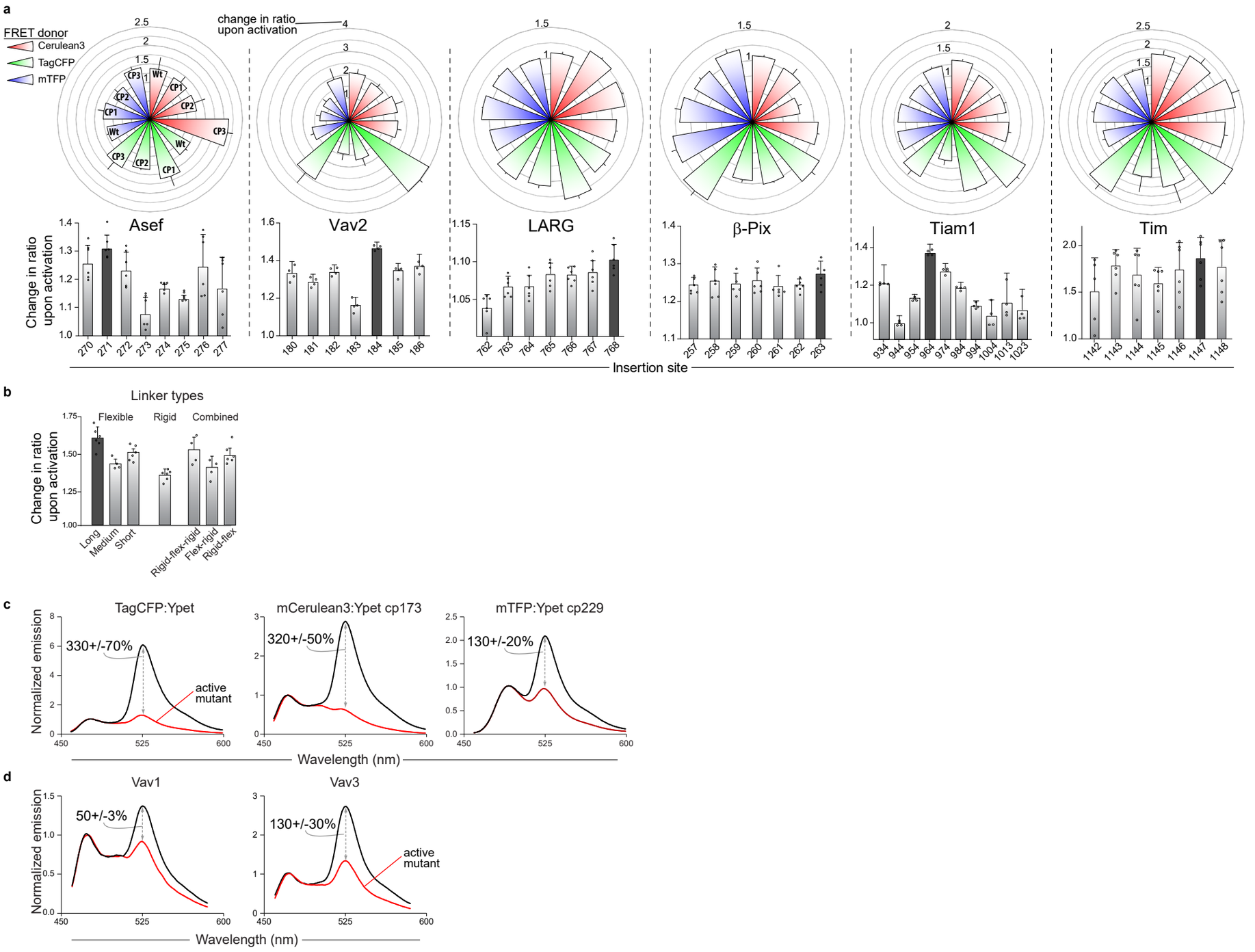

(a) Screening RhoGEF biosensor designs. For each RhoGEF: Upper - Screening donor (wedge color) and acceptor (Wt – YPet; CP1 – YPet CP157; CP2 - YPet CP173; CP3 – YPet CP229) fluorophore combinations. (n=3). Lower - Screening different insertion sites for the fluorescent protein cassette (Asef, n= 6; Vav2, n= 4; LARG, n=6; β-Pix , n=6; Tiam1, n= 4; Tim, n= 6). (b) Comparison of different donor to acceptor linker compositions for the Vav2 biosensor (n=6). a, b - Bars represent mean of n independent transfections across multiple experiments. Error bars are 95% C.I. (c) Emission spectra of the Vav2 variant with the highest dynamic range for each donor. Donor/FRET emission ratio change between active (Y142E:Y159E:Y172E:Δ860) and wild type conformations is indicated, ex = 430nm. (n=9 independent transfections, +/- 95% C.I.) (d) Emission spectra of biosensors for Vav1 and Vav3. Donor/FRET emission ratio change between active (Vav1 - Y142E:Y160E:Y174E, Vav3 - Y160E:Y173E) and wild type mutants, ex = 430nm). (Vav1 n=4, Vav3 n=6 independent transfections across multiple experiments, +/- 95% C.I.)

Supplementary Figure 2

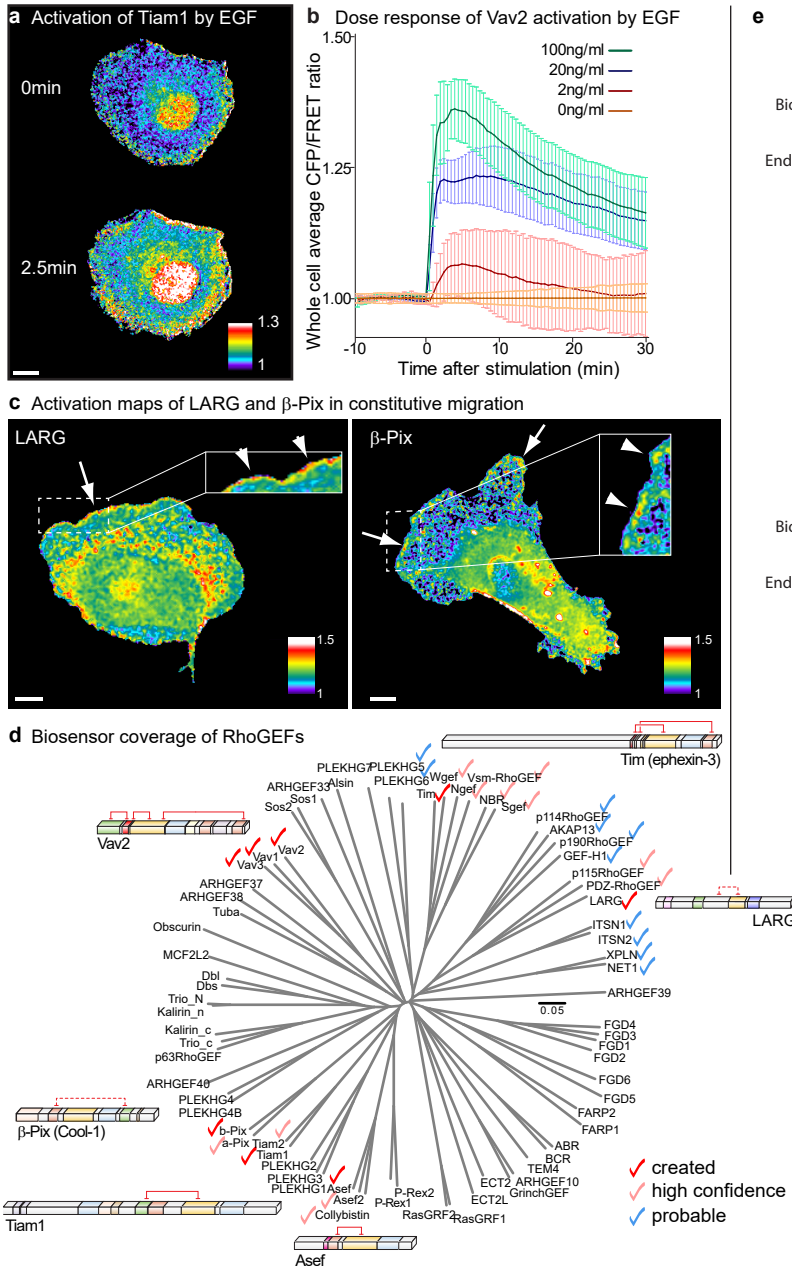

(a) A431 cells expressing Tiam1 biosensor after stimulation with EGF (100ng/μl). Donor/FRET ratio images pseudo-colored with scale bar at bottom right. (b) Whole cell average Donor/FRET ratio of A431 cells expressing the Vav2 biosensor before and after stimulation with the indicated concentrations of EGF. Graphs are average of 10 cells per concentration, error bars indicate 95% confidence intervals. (c) LARG (left) and β-Pix (right) activation reported by biosensors in MDA-MB-231 cells undergoing serum-dependent constitutive edge motion. Arrows point to activity in protrusions. Boxed regions show magnified images, arrowheads show activity at edge. a, c -images representative of three independent experiments. Pseudocolor as in Fig. 1. Scale bars 10μm. (d) DH family RhoGEFs amenable to biosensor production through modification of the hinge region. (e) Uncropped scan of whole blots from Figure 1c.

Supplementary Figure 3

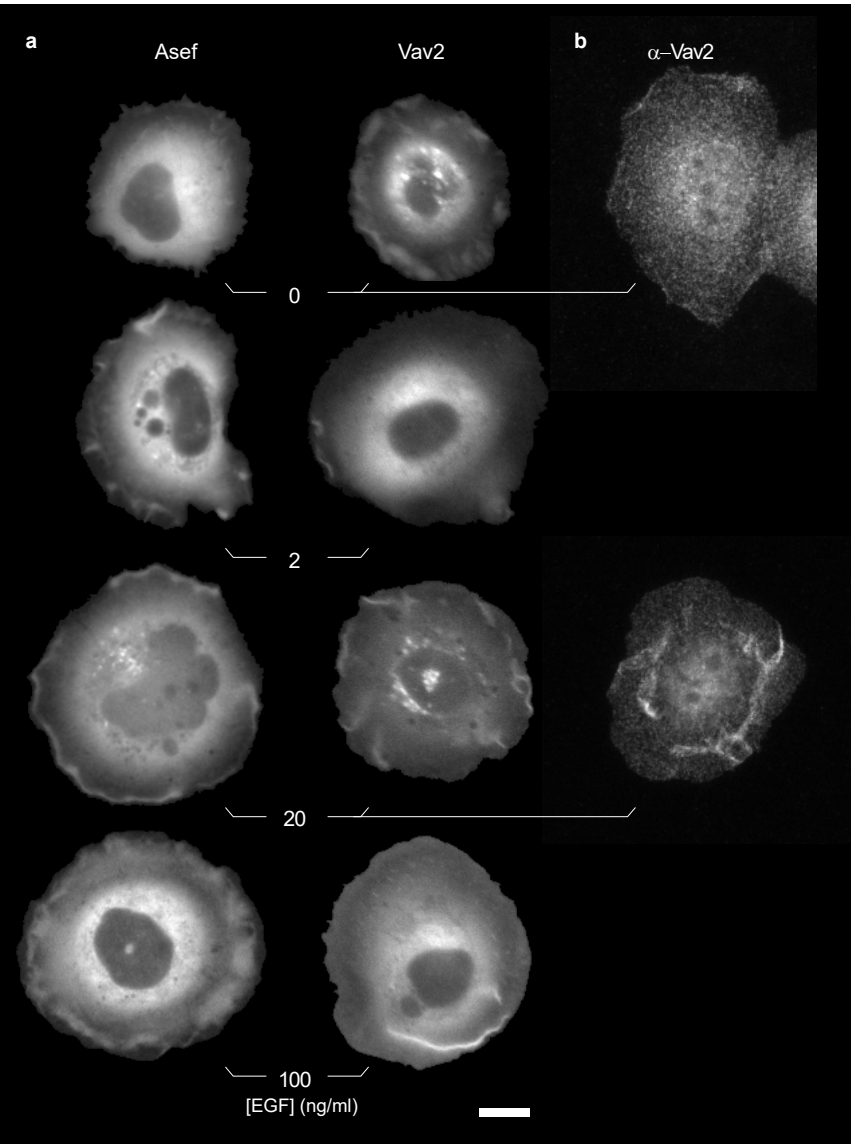

Biosensor localization in EGF stimulation experiments. (a) Donor emission of cells from Figure 1d showing biosensor localization. (b) Localization of endogenous Vav2 in A431 cells after EGF stimulation. Images representative of three independent experiments. Scale bar 10µm.

Supplementary Figure 4

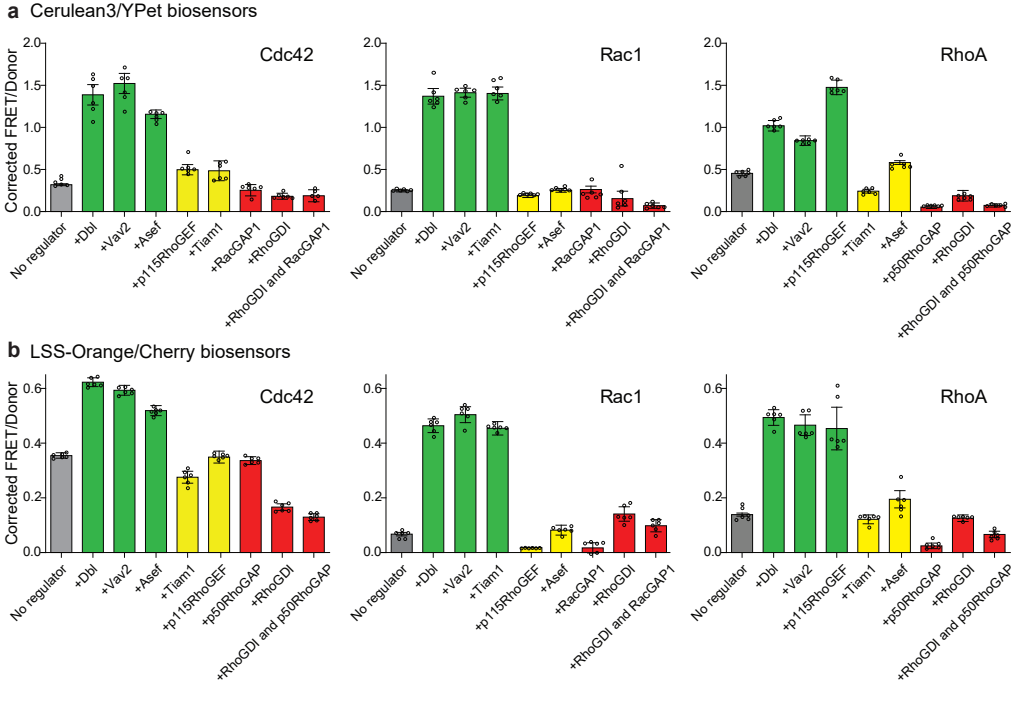

Response to upstream regulators of GTPase biosensors using Cerulean3/YPet (a) and LSS-Orange/Cherry (b) FRET pairs. Bars indicate FRET/donor ratio upon co-expression of each regulator with the biosensor. Green bars represent positive regulators, red bars negative regulators and yellow bars are RhoGEFs that should not directly activate. Bars represent mean of 6 independent transfections across multiple experiments. Error bars are 95% C.I.

Supplementary Figure 5

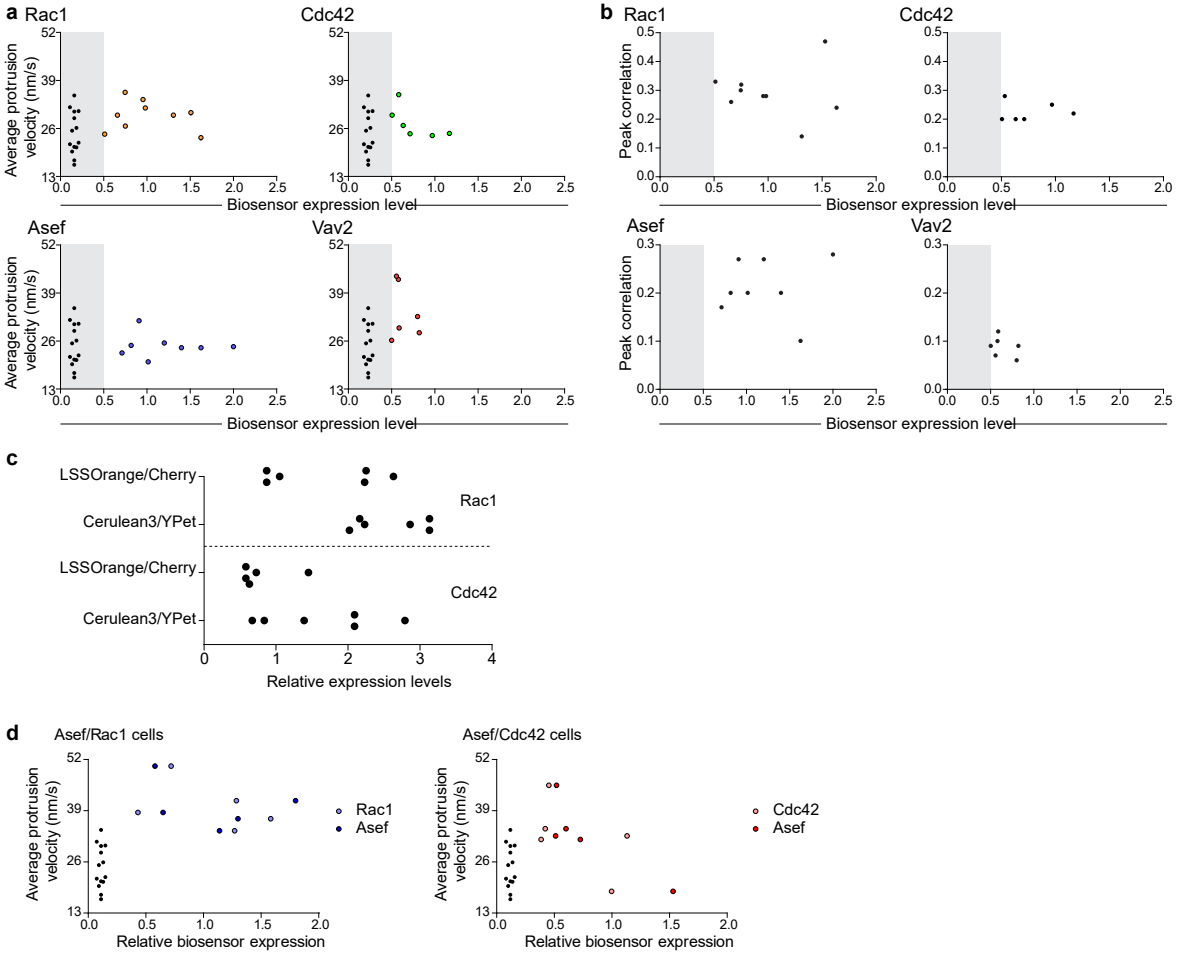

Relationship between biosensor expression level and average protrusion velocity (a) or peak correlation with edge velocity (b). No significant relationship was detected between biosensor expression level and velocity. Expression levels were determined relative to the fluorescence of the medium in the shade-corrected FRET image. The grey box at left of each graph indicates expression levels where the SNR is too low for FRET analysis. The black dots within the grey box show the velocities for control cells expressing only mCherry-CAAX (c) Comparison of GTPase biosensor expression using Cerulean3/YPet and LSSOrange/mCherry based biosensors. Relative expression was calculated using donor brightness, adjusting emission intensity for differences in the dichroic, emission filter, protein brightness and camera efficiency at the different wavelengths (data obtained from fpbase.org). (d) Relationship between biosensor expression level and average protrusion velocity for cells expressing two biosensors. No significant relationship was detected between biosensor expression level and velocity at these expression levels.Data representative of at least 3 independent experiments.

Supplementary Figure 6

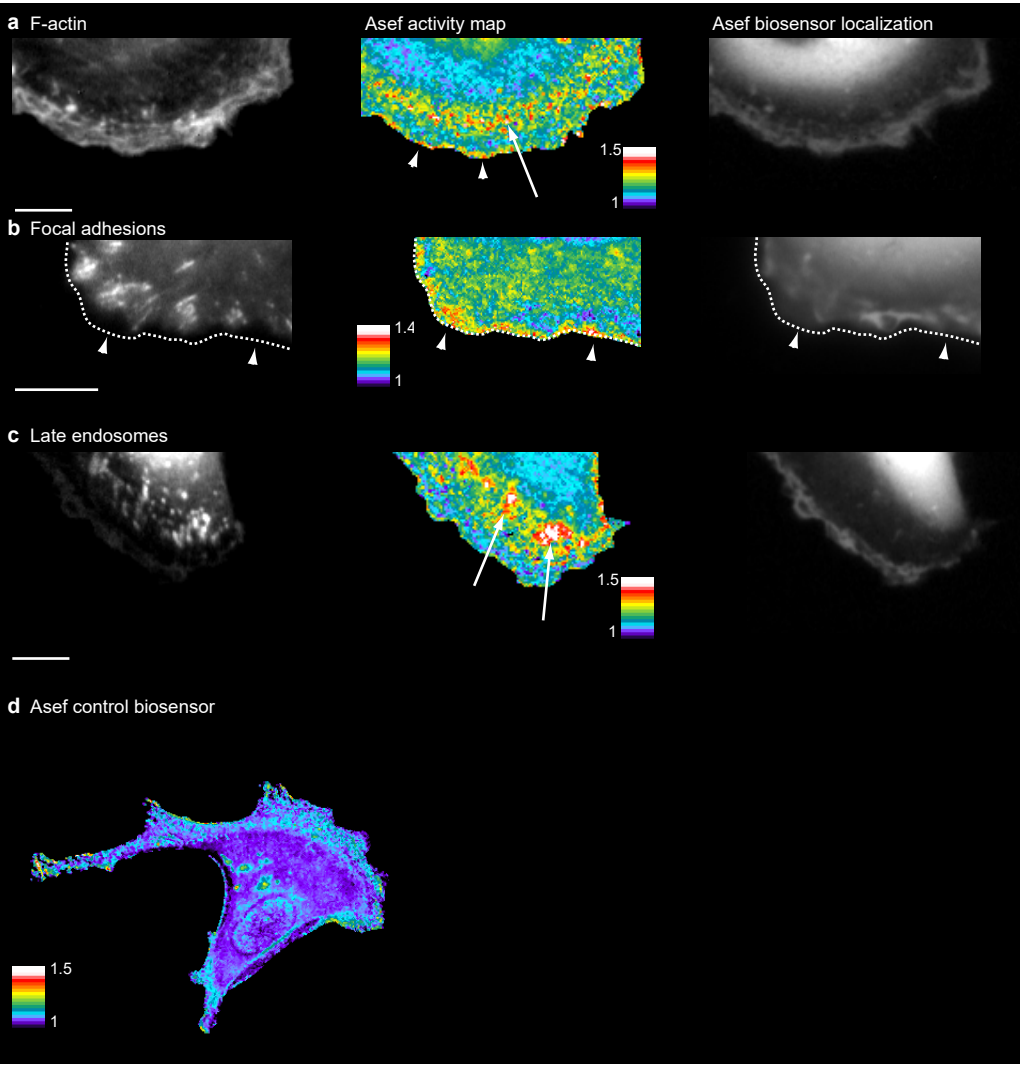

(a-c) Asef activation (middle) reported by biosensors in MDA-MB-231 cells undergoing constitutive protrusion-retraction cycles. Cells co-express markers (left) labelling (a) F-Actin (F-tractin), (b) Focal adhesions (Paxillin, acquired using TIRF illumination), and (c) Late endosomes/sorting components (Rab7). Arrowheads point to activation at the edge, Arrows point to second layer for Asef that lies behind lamella/adhesion zone. Right shows biosensor donor emission. (d) Control biosensor for Asef shows greatly reduced ratio across the cell. Activity maps pseudocolor as in Fig. 1. Scale bars 10μm. Images are representative of at least 3 independent experiments.

Supplementary Figure 7

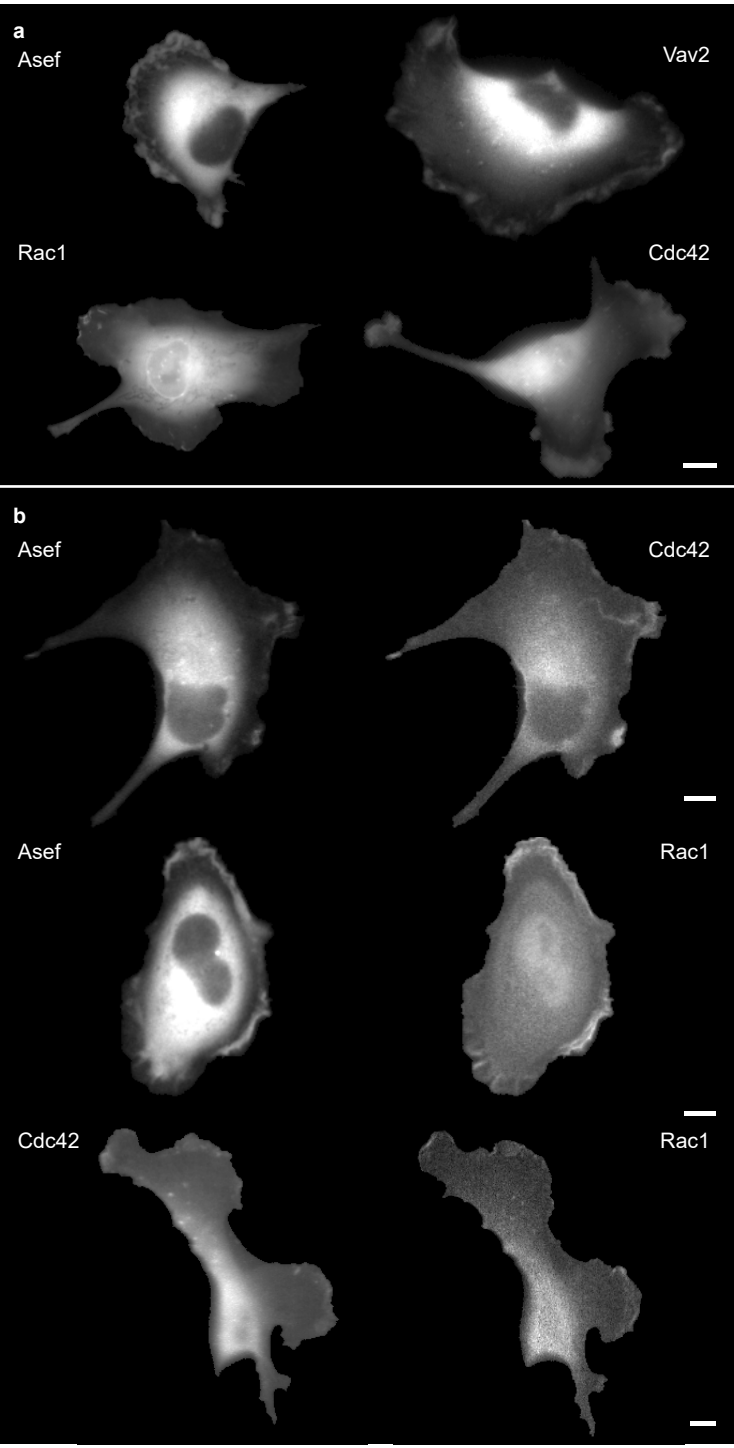

Biosensor localization in cell with constitutive edge protrusion-retraction cycles. (a) Donor emission of cells from Figure 3 showing localization of biosensor. (b) Donor emission of cells from Figure 5 showing localization of biosensor. Images are representative of at least 3 independent experiments.

Supplementary Figure 8

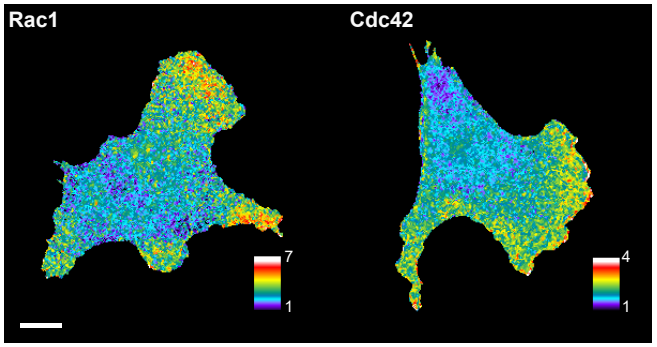

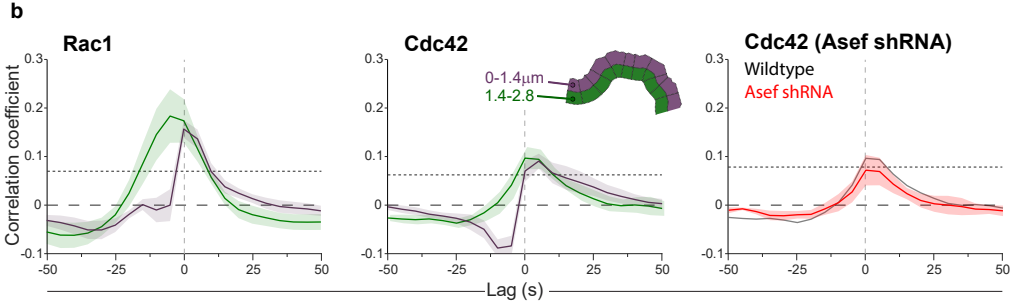

(a) Rac1 and Cdc42 activation reported by red-shifted biosensors in MDA-MB-231 cells undergoing random edge motion. Pseudocolor as in Fig. 1. Scale bars 10μm. Images are representative of at least 3 independent experiments. (b) Average Pearson's cross-correlation functions for red-shifted GTPase biosensors. Analysis using 1.4 μm window size. (n = cells, m = windows); Rac1 (left, n=10, m=788); Cdc42 (middle, n=7, m=990, inset shows window color key.); Cdc42 in Asef shRNA cells (right, red, 1.4-2.8 μm layer, Cdc42 correlation for wildtype cells is shown in grey; n=5, m=625). Inset shows window size and color key. Dotted lines show the correlation coefficient above which the coupling between two variables is considered significant with 95% confidence. This depends on the number of windows (see Methods). Shading represents 95% C.I. about the mean correlation computed from m windows. The width of this interval depends on the consistency of the correlations across windows and cells (see Methods).

Supplementary Figure 9

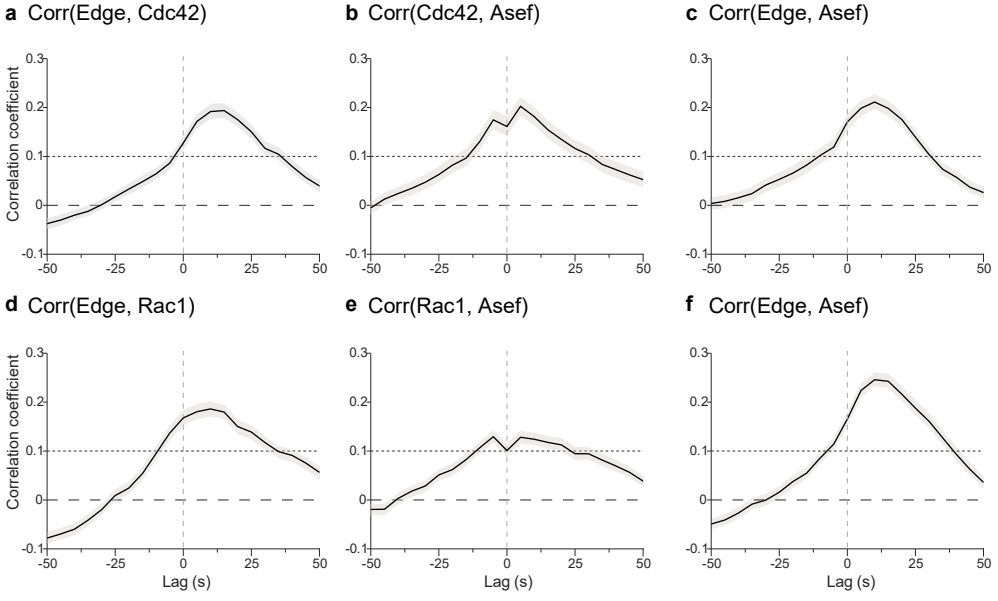

Average Pearson's cross-correlation functions for each combination of edge, RhoGEF activity, and Rho GTPase activity for each biosensor pair ((a-c) Asef and Cdc42 (n=6, m=729), (d-f) Asef and Rac1 (n=6, m=719). Analysis using 1.4 m window size, 1.4-2.8μm layer. Dotted lines show the correlation coefficient above which the coupling between two variables is considered significant with 95% confidence. This depends on the number of windows (see Methods). Shading represents 95% C.I. about the mean correlation computed from m windows. The width of this interval depends on the consistency of the correlations across windows and cells (see Methods).

Supplementary Figure 10

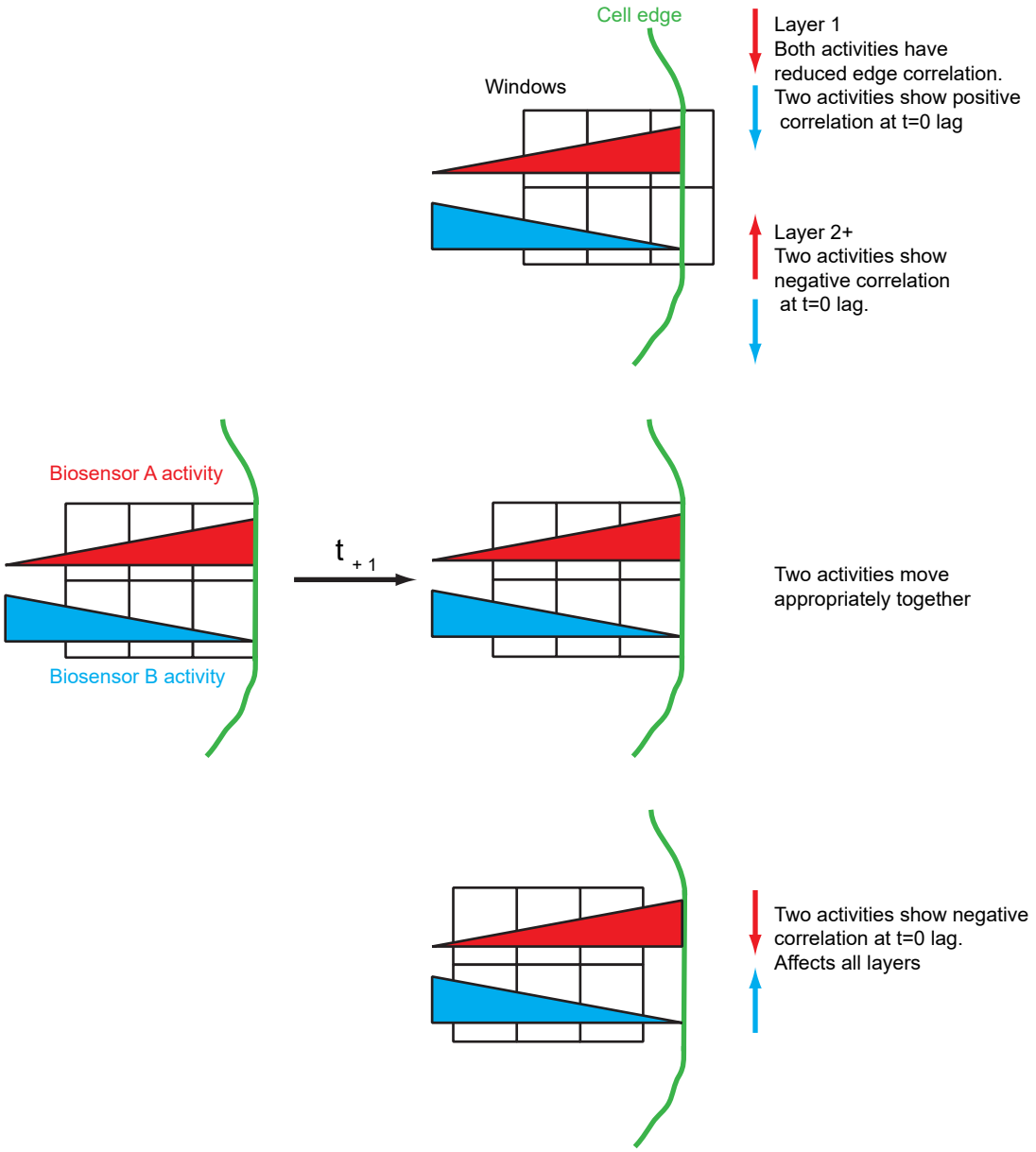

Diagram to illustrate potential artefacts caused by sub-pixel errors in segmentation of biosensor images when two biosensors have inverse gradients.

Thorough investigation unveiled an unfortunate systematic amplification of subpixel errors in the cell edge segmentation and window positioning that yields a depression of the correlation values specifically at zero time lags. When edge is correctly assigned (middle) the biosensor activity is correctly measured and the cross correlation is correctly measured. When the first window edge extends onto non-cell areas (top), both activities are low in the first window, so giving an incorrect positive correlation. In layer 2 and deeper, biosensor A (red) is artificially high, while biosensor B (blue) is low, giving a negative correlation at lag=0. When the first window edge fails to extend to the cell edge (lower), biosensor A (red) is artificially low, while biosensor B (blue) is high in all layers, giving a negative correlation at lag=0. The effect is strongest in the second window layer because of the inverse spatial gradients in RhoGEF and GTPase activity (RhoGEF activity increases with distance from the edge; GTPase activity decreases with distance from the edge). At this point, there is no remedy for this effect, though improvements in resolution and segmentation could ameliorate it.

Supplementary Figure 11

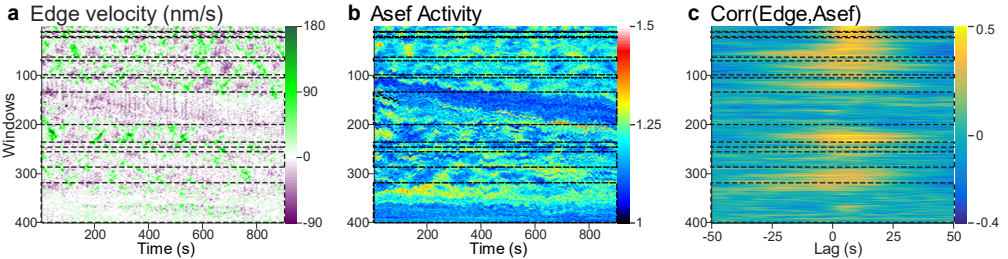

Comparison with Figure 2, showing excluded quiescent windows. (a) Map of edge velocity along the edge. Green regions are protruding, purple regions retracting. (b) Map of Asef activity along the edge. Red/yellow regions have high activity, blue regions have low activity. (c) Cross correlation coefficients between edge velocity and Asef activity. Gold shows high correlation, blue negative correlation. (a-c) Each column is a single time point along the edge, each row is a single position through time. Black boxes show quiescent regions that are excluded.

Supplementary Movie Captions

Supplementary Movie 1.

Cdc42 (left) and Rac1 (right) activation reported by biosensors in MDA-MB-231 cells undergoing random edge motion. Pseudocolor as in Fig. 1. Movies are representative of at least 3 independent experiments.

Supplementary Movie 2.

Asef (left, middle) and Vav2 (right) activation reported by biosensors in MDA-MB-231 cells undergoing random edge motion. Enlarged view on left shows activation of Asef at cell edge. Pseudocolor as in Fig. 1. Movies are representative of at least 3 independent experiments.

Supplementary Movie 3.

Simultaneously imaged RhoGEF and Rho GTPase biosensors in MDA-MB-231 cells undergoing constitutive edge motion. Upper images show activation of Asef (left) and Cdc42 (right), lower images show Asef (left) and Rac1 (right). Pseudocolor as in Fig. 1. Movies are representative of at least 3 independent experiments.

Supplementary Movie 4.

Simultaneously imaged Cdc42 and Rac1 biosensors in MDA-MB-231 cells undergoing constitutive edge motion. Pseudocolor as in Fig. 1. Movies are representative of at least 3 independent experiments.